Journal of
Micromechanics and
Microengineering

TECHNICAL NOTE

Embedded electrohydrodynamic printing of magnetically responsive microspheres

To cite this article: Prashant Ghimire *et al* 2026 *J. Micromech. Microeng.* **36** 077001

Journal of Micromechanics and Microengineering

RECEIVED
18 January 2026

REVISED
24 March 2026

ACCEPTED FOR PUBLICATION
10 June 2026

PUBLISHED
1 July 2026

TECHNICAL NOTE

Embedded electrohydrodynamic printing of magnetically responsive microspheres

Prashant Ghimire[1], Augustus Kitchens[1], Kishwat Ijaz Malik[2], Yueheng Lin[1], Yongjian Qiu[3], Yang Cao[2,*] and Yiwei Han[1,*]

[1] Department of Mechanical Engineering, University of Mississippi, University, MS, United States of America
[2] Department of Mechanical and Industrial Engineering, Montana State University, Bozeman, MT, United States of America
[3] Department of Biology, University of Mississippi, University, MS, United States of America
[*] Authors to whom any correspondence should be addressed.

E-mail: yang.cao1@montana.edu and yhan2@olemiss.edu

Keywords: electrohydrodynamic (EHD) printing, embedded printing, microspheres, magnetically responsive, magnetic microspheres

Supplementary material for this article is available online

Abstract

Magnetic microspherical robots have promising applications in targeted drug delivery and microsurgery. Due to the high droplet impact speed on the conventional substrate, microspheres are very challenging to print. In this study, we integrate electrohydrodynamic (EHD) printing and mineral oil-based bath materials to develop a novel embedded EHD printing to direct print polydimethylsiloxane–iron microspheres. The comparison results between conventional EHD printing and embedded EHD printing show that microspheres can be directly produced from embedded EHD printing, and the bath material can enhance the electric field confinement, which significantly lowers the required printing voltage. A study is carried out to understand the effect of two major printing parameters, voltage and pressure, on the feature resolution. Scanning electron microscopy images confirm the geometric shape of the printed microspheres, and magnetic tests demonstrated the propulsion and navigation of these magnetic microspheres. These findings demonstrate the potential of fabricating microspheres using this novel embedded EHD printing approach, providing an important insight towards the manufacturing of soft robotics, adaptive sensors, and targeted microsystems.

1. Introduction

Magnetic microrobots are microscale soft robotics driven by magnetic fields. They can be wirelessly navigated to hard-to-reach, confined, and delicate inner body sites for a range of biomedical applications, such as minimally invasive surgery [1–3], targeted drug delivery [4–7], and tissue engineering [8–11]. As a typical form of magnetic microrobots, spherical magnetic microrobots or magnetic microspheres are known for their simple structure and locomotion versatility [12]. When actuated by a rotating magnetic field, magnetic torque tends to align the magnetic microsphere's magnetic moment with the direction of the rotating magnetic field, causing it to roll on a surface. Despite its rapid progress, the performances and applications are still limited by the available fabrication approaches. A simple and reliable fabrication approach that can create high-resolution structures with controlled material compositions and certain properties is critical for achieving precise control and predictable movement under magnetic fields. Currently, most of the composite material-based microrobots are in the range of several millimeters to several hundred microns, and the manufacturing of smaller size microrobots usually includes a series of complex processes, which are time-consuming and costly [13].

Additive manufacturing (AM) is a bottom-up process in which the object is created layer by layer. AM expands the design space for complex objects, enables exploration of new material properties, and may eventually change how we configure both local and global supply chains [14]. Although different 3D printing processes like stereolithography [15], powder bed fusion [16], direct ink writing

(DIW) [17], and fused deposition modeling [18] have been in effective use for a long time, some major challenges still exist. Many functional materials need to have either rapid solidification properties or self-supporting properties after printing to keep their shape or their functions, which creates a barrier for material selection [19–22]. For instance, high-resolution spherical droplets or particles, which have unique advantages to be used in drug delivery, surface coating, soft robotics, and bio-medics [23, 24], are extremely difficult to be directly produced by traditional AM processes due to the inherent limitations of the processes or the unavoidable presence of the substrate. In nozzle-based printing technologies, the substrate is an essential component on which droplets will be directly deposited. It is impossible to maintain a spherical droplet once it impacts and spreads on the substrate. Even on a surface-treated substrate, a small flat surface at the contacting area is still unavoidable.

Recently, embedded printing technology has been developed for biomedical and tissue engineering [25, 26]. In this process, 3D structures are directly printed inside a yield-stress bath material [27, 28] instead of on a substrate. The yield-stress bath material acts as a supporting medium, where the nozzle moves around for printing and rapidly recovers its intact solid-like phase once the nozzle passes, so that the printed ink remains bonded, preserving the desired printed shape. This bath material will support the printed 3D structures until the completion of the printing process; thus, the shape of the printed structures will not be altered. Upon curing and solidification, the printed structures can be extracted from the bath material and undergo postprocessing as required. Up to date, most of the embedded printing approaches are based on integrating extrusion printing and supporting bath materials, where the printing materials will be directly extruded from the nozzle into a yield-stress bath to form the 3D structures by pressure. Gao *et al* used a very high pressure of 80 kPa to extrude the ink inside the bath composed of Pluronic F-127 for bioprinting [29]. Grosskopf and his team used viscoplastic matrix materials to print the structures and studied the effect of print speed and nozzle size on the yield dimensions when the fluid is flowing around a cylinder nozzle. They successfully printed the spiral structures with a diameter of 0.72 mm [30]. A group of researchers led by Truby used a 25 wt% suspension of physically gelled Pluronic F127 in deionized, ultra-filtrated water as the bath material to fabricate a soft somatosensitive actuator innervated with multiple soft sensors to maintain their printed shapes [31]. Luo *et al* used a biocompatible support as the pregel solution to overcome the difficulty of printing the aqueous microstructures, as they generally tend to alter the printed shape due to surface tension. They printed different freestanding shaped structures of various shapes, like springs, barbells, tornadoes, etc [32]. One review paper has mentioned the approach of using the embedded 3D printing along with a detailed classification of different types of bath materials that are being used for different purposes, especially in bioengineering and drug delivery. They have also explained about the general ink materials compatible with different supporting baths to print a fully functional component after the deposited ink is fully cured [33]. The printed results of these extruded embedded printing are generally of low resolution due to the mechanisms of the process, in which the nozzle size determines the resolution of the printed features. A smaller nozzle can be implemented to improve the resolution for fabricating microscale structures for micro-electromechanical systems or bioengineering systems, but it requires impractical pressure that is difficult to achieve. In addition, a smaller nozzle brings a higher chance of getting clogged. Due to these restricting mechanisms of the extrusion-based embedded printing processes, it is very challenging to create high-resolution 3D objects or structures, so a new process is needed to fulfill the needs for printing of microscale features.

Electrohydrodynamic (EHD) printing is a versatile, high-resolution printing technique [34]. Unlike inkjet printing or DIW, EHD printing is driven by an electric field that is present between the substrate and the nozzle. The electric field drives charge carriers in the ink toward the substrate. When the electrostatic force overcomes the surface tension of the liquid, a Taylor cone is created at the tip of the nozzle with the ejection of nanodroplets or a fine cone-jet. Interestingly, the ejected jet or droplet is of the order of one magnitude smaller than the nozzle diameter, allowing for high-resolution material deposition [35–37]. In addition, EHD printing can process various materials, which makes it one of the promising printing techniques to fabricate high-resolution functional structures. However, our previous studies have shown that the droplet possesses a very high speed when impacting the substrate [38, 39]. As a result, the droplet will spread on the substrate and form a hemispherical structure, and spherical droplets or particles cannot be created using EHD printing.

Herein, a novel embedded EHD printing has been developed to address those challenges by submerging an EHD printhead into a bath material. To the best of our knowledge, no such printing method that is capable of directly producing microspheres in a single process has been reported. In this work, we have characterized the two main printing parameters in the embedded EHD printing process and utilized this process to successfully fabricate magnetic microspheres. We have demonstrated excellent propulsion

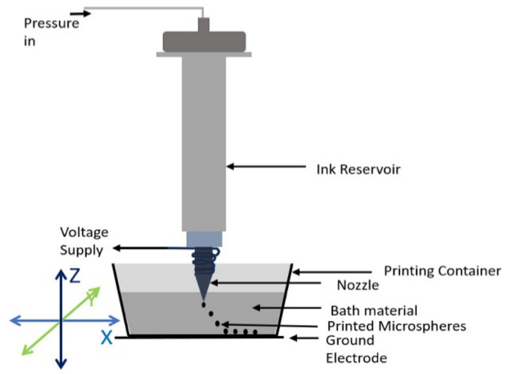

Figure 1. Experimental setup for EHD embedded printing.

and navigation performance of printed magnetic microspheres, which shows promising future applications of applying embedded EHD printing to fabricate microspheres in biomedical and bioengineering applications.

2. Method

2.1. Embedded EHD printing setup

The embedded EHD printing system that is shown in figure 1 consisted of a three-axis (*XYZ*) precision stage (V-508, PI-USA), printhead, voltage supply (Trek-610E), pressure system, and a printing bath. The printhead includes a syringe with a metallic nozzle at the tip. A rounded transparent glass container with a diameter of 29.36 mm was used to hold the bath material. A high voltage was connected to the nozzle, and the ground electrode was placed under the glass container. The 3D precision stage was used to control nozzle movement with a 50 nm accuracy and repeatability. Compressed air with a maximum pressure of 90 psi was used to control the flow rate of printing material. The voltage supply can provide a voltage up to 10 kV. A high-resolution camera set with 1 μm resolution was used to monitor and record the printing process. In the experiment, two nozzle sizes have been used. Non-coated, nickel silver precision core nozzles (Subrex) with inner and outer diameters of 0.057 mm and 0.169 mm, respectively, were used to characterize the embedded EHD printing. A standard 22-gauge nozzle (inner diameter: 417 μm, outer diameter: 720 μm) was used to produce larger droplets for better sample handling and operating for scanning electron microscopy (SEM) imaging and magnetic testing.

2.2. Polydimethylsiloxane (PDMS)-Fe printing ink and fluid bath preparation

PDMS (Dowsil SYLGARD 184 Silicone Elastomer Kit, Dow Corning) solution was first prepared by mixing it with the curing agent at a ratio of 1:10. Then, the iron (Fe) nanoparticles (99.7%, particle diameter: 100–130 nm, Sky Spring Nano materials) were added onto the mixture of the PDMS and curing agent. A sonicator was used to disperse the Fe nanoparticles, and the mixture was then stirred for 15 min to even distribute the nanoparticles within the mixture. The printing ink, with a volume ratio of 1:10 of Fe particle to PDMS, was synthesized, and its viscosity was characterized with a rotational viscometer (Model: NDJ-5S). The measured ink viscosity is 11 437 cP at a shear rate of approximately 6 s^{-1}, which can provide a suitable flowability for a stable embedded EHD printing. The viscosity of the PDMS/Fe ink was characterized with a rotational viscometer (Model: NDJ-5S). Mineral oil (EmbryoMax, Filtered Light Mineral Oil, Sigma Aldrich) was mixed in polyvinyl alcohol (PVA) (87%–90% hydrolyzed, average mol wt. 30 000–70 000, Sigma Aldrich) at 4% (w/w) and kept still for 10–15 min before printing. The added PVA was used to tune the viscosity [40, 41] and surface tension of the bath, which will help to improve the stability of the printing process and prevent the printed droplet from settling down at the bottom before it cures [42]. The bath material was loaded into a transparent glass container in which the magnetic microspheres will be printed.

2.3. Embedded EHD printing process characterization

In EHD printing, the applied voltage and pressure have been identified as two of the most critical parameters that influence the printing behavior and printing stability. However, in the embedded EHD printing, the surrounding environment (bath) also plays an important role in determining the printing behavior. In conventional EHD printing, the nozzle was surrounded by air, whereas in the embedded EHD printing, the nozzle was immersed in a bath material. To study the effect of the bath on EHD printing, two different environmental media, air (the media used in conventional EHD printing) and a mixture of mineral oil and PVA, were selected. When printing in the air, a traditional EHD setup used in our previous work was applied [43]. The applied voltage used for printing the ink in the air was between 0.25 kV and 2 kV, whereas the voltage used for printing inside the bath was from 0.25 kV to 0.55 kV. A pressure from 2.5 psi to 4.5 psi was applied in both cases. The standoff distance (the gap between the nozzle and the substrate) was maintained at 4 mm, and the printing speed was set to 0.5 mm s^{-1}. A high-resolution camera was used to observe the printing process.

2.4. Optical and SEM imaging

The dispersion of the Fe nanoparticles within the PDMS matrix and the morphology of the printed magnetic microspheres were observed under an optical microscope and SEM. To study the distribution of the Fe nanoparticles, a droplet was first printed onto a glass slide using the conventional extrusion process. Optical microscope images were then collected to evaluate the dispersion of Fe nanoparticles within the PDMS. To study the morphology of the printed m magnetic microspheres, the glass container was transferred from the printing stage to the optical microscope immediately after printing. The printed magnetic microspheres were viewed and measured directly using the microscope software. For SEM imaging, a 22-gauge nozzle was first used to print magnetic microspheres with a size ranging from 270 μm to 820 μm. The printed magnetic microspheres were allowed to stay in the glass container for four days to get fully cured before being taken out and placed on a substrate. The cured droplets were washed multiple times with water and ethanol to make sure that they were free of dust and other particles. The cured magnetic microspheres were then coated with a thin platinum layer to improve the conductivity of the sample surface. The printed magnetic microspheres were placed on a glass substrate and put in a sputtering coater for 30 s. The samples were flipped on the substrate for a second time, coating for 30 s, to ensure all surfaces of the droplet were coated with platinum. A carbon conductive tape was placed between the SEM sample holder and the coated magnetic microspheres. The accelerating voltage and working distance of the SEM were set to 5.0 kV and 7 mm, respectively.

2.5. Preparation of magnetic microspheres and magnetic testing

To verify the propulsion and navigation of the printed magnetic microspheres, magnetic microspheres of different sizes were printed with the 22-gauge nozzle. The printed magnetic microspheres were left in a glass container for four days to get fully cured before being transferred to a filter paper (pore size of 25 μm), using a glass micropipette of diameter 1 mm made from the micropipette puller machine (Sutter instrument, model P-1000) to remove the residual mineral oil from the bath. Then the filtrate (magnetic microspheres) was shifted to a transparent container for cleaning. A three-axis Helmholtz magnetic coil system was built to test the propulsion and navigation of the magnetic microspheres. A LabVIEW program allows the user to define the magnetic field flux density, frequency, and axis of rotation, by which the program then determines the corresponding voltage signal for each pair of coils. The magnetic coil system can provide a magnetic field with a strength up to 5 mT and frequency up to 50 Hz that rotates along an arbitrary direction.

3. Results and discussion

As mentioned above, the Fe nanoparticle distribution within the PDMS matrix was first studied with optical images. As shown in figure 2, the nanoparticles appear to be well dispersed throughout the PDMS matrix, with no obvious large cluster observed. Based on the well-dispersed ink formulation, the printing behaviors under both conventional EHD printing and embedded EHD printing were further investigated. In conventional EHD printing, air is the surrounding medium, and the behavior and shape of liquid droplets are determined by the interplay between electrostatic forces and surface tension. When a droplet is exposed to an electric field, free charges gather at the liquid–air boundary, creating Maxwell stresses that tend to stretch the droplet in the direction of the applied field. Conversely, surface tension works to minimize the surface area and thus opposes deformation, preventing the formation of the droplet. The equilibrium between these forces is crucial in determining the formation of the droplet. In this work, when applying a voltage of 0.5 kV and a pressure of 5 psi, no droplets were

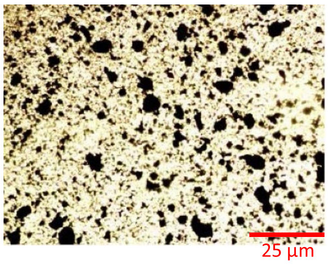

Figure 2. Optical microscopy image of Fe nanoparticles dispersed within the PDMS matrix.

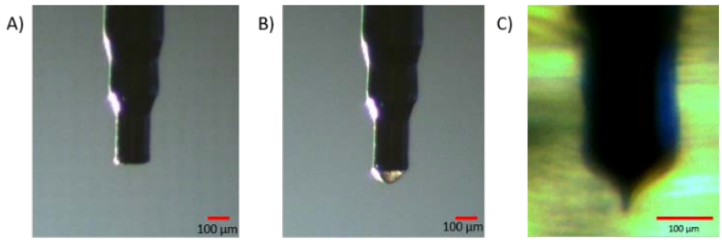

Figure 3. (a) Nozzle without discharge at 5 psi and 0.5 kV in traditional EHD setup (air) (b) Taylor cone formed at 2 kV at 5 psi in air (c) Taylor cone formation after reaching a critical voltage (0.25 kV) inside the mineral oil bath.

ejected from the nozzle (figure 3(a)). Even with a higher voltage of 2 kV, only a meniscus formed at the nozzle tip (figure 3(b)), which indicated a weak electric field [44]. The weak electric field cannot generate enough electrostatic force to overcome the surface tension force to deform the meniscus into a Taylor cone and produce droplets. However, when the nozzle is placed into the mineral oil-based bath media, droplets can be ejected with a lower voltage and pressure, as shown in figure 3(c). This can be explained by the fact that the surrounding bath ($\varepsilon \approx 2.3$) has a higher dielectric constant and viscosity than air ($\varepsilon \approx 1.0$), which changes the electric field distribution and intensity around the nozzle. The bath material with the higher permittivity enables the focus of the electric field intensity near the meniscus [45], which allows more charges to accumulate at the tip of the meniscus, allowing an easier cone formation; thus, the droplet can be ejected in the bath material using printing parameters comparable to or lower than the required value in the conventional EHD printing. The viscous, insulating medium increases the charge relaxation time, permitting electrostatic pressure buildup sufficient for droplet emission [46]. In addition, compared with the conventional EHD printing, the low interfacial tension between the printing ink and bath material will also assist the ink breakup and droplet formation.

To further understand the embedded EHD printing, we have studied the effect of the voltage and pressure on the embedded EHD printing process, as both parameters will contribute to the ink flow and feature resolution. A process characterization has been performed for both voltage and pressure. Four different pressures (3 psi, 3.5 psi, 4 psi, and 4.5 psi) and four different voltages (0.25 kV, 0.30 kV, 0.35 kV, and 0.40 kV) were applied in the tests. When the pressure is less than 3 psi, the system cannot discharge any material out of the nozzle.

To characterize the voltage, the nozzle was first dipped inside the printing bath, where no discharge was seen at the tip of the nozzle, as shown in figure 4(a), within the pressure range as discussed earlier. The meniscus can only be seen if the pressure is increased to a value above 10 psi, but still very difficult to generate the droplet and separate from the nozzle unless the voltage is applied. This can be easily explained as the air pressure cannot overcome the surface tension between the ink and the nozzle, and the pressure from the bath material. When gradually increasing the voltage to just below 0.25 kV, only a cone shape was formed at the nozzle tip. Adding voltage will generate a focused electric field around the nozzle, creating a strong electrostatic force, which will pull the ink out from the nozzle and form the cone shape. However, when the applied voltage does not generate sufficient electrostatic force to overcome the surface tension force and pressure force from the bath, the droplet cannot be ejected.

After increasing the voltage to 0.25 kV, a Taylor cone was formed, and a droplet was ejected. Under this condition, the voltage can provide enough force to break the ink surface tension and bath pressure acting on the tip of the cone, thus, the droplet detached from the cone. Figure 4(b) shows the result of

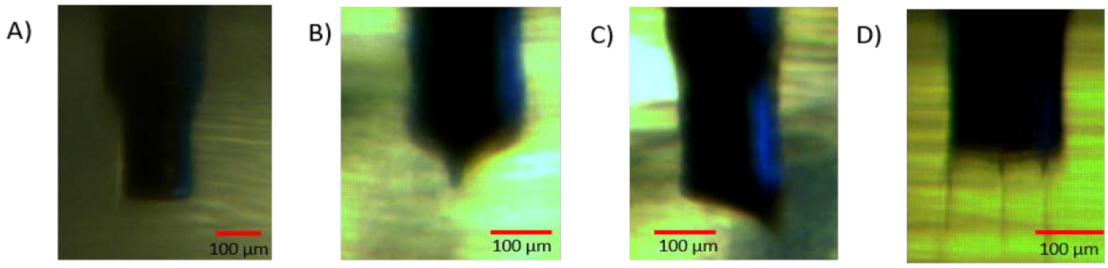

Figure 4. Nozzle discharge modes of embedded EHD printing. (a) Nozzle without discharge before a critical voltage is reached. (b) Taylor cone formation after reaching a critical voltage. (c) Unstable jet being formed after voltage increment. (d) Multijet formation after voltage is sufficiently increased.

the Taylor-cone shape at the nozzle tip when the voltage was applied. When continuing to increase the voltage from 0.25 kV to 0.40 kV, droplets of different sizes can be obtained. In this voltage range, micro-scale droplets with uniform size were formed and ejected from the nozzle. Figure 5(a) shows the relation of droplet diameter and applied voltage at different pressure values ranging from 3 psi to 4.5 psi. Figure 5(b) shows the optical images of the printed microsphere with different voltages under a constant pressure of 4.5 psi. Generally, a decrease in the droplet diameter has been seen with the gradual increase in the voltage across the pressure values. Increasing the voltage will increase the electric field strength around the nozzle, which reduces the electrostatic stretching of the ink jet and requires volume of the printing ink to provide enough charges and forces to separate the ink from the nozzle, thus encouraging finer breakup with smaller droplet formation. Under this printing condition, droplet size and location can be controlled, as each time only a single droplet was printed. In addition, due to the viscosity of the bath material, the printed droplets can remain suspended in the bath without settling down to the bottom of the container, which provides an ideal environment for forming the spherical shape. Figure 5(c) shows the microsphere size distribution at different voltages under a constant pressure of 4.5 psi. The results clearly showed that all of the printing conditions were able to produce uniform microspheres with a variance of within 3 μm, demonstrating a good control over droplet formation and high reproducibility of the embedded EHD printing process. In addition, the smallest droplet diameter of 19 μm from a stable printing was obtained under a voltage and pressure of 0.4 kV and 4.5 psi, with over 80% of the microspheres concentrated at this size, indicating a highly stable printing process. The results also showed that the blended effect of the higher pressure and voltage can give the smallest result. Moreover, higher voltages and higher pressures are able to reduce the variance in the droplet size, stabilize the breakup process, and yield more uniform droplets.

As the voltage increased further to above 0.45 kV, the formed cone is slowly shifted to one side of the nozzle with smaller drops and increased jetting speed as depicted in figure 4(c). Moreover, this skewed cone showed slow oscillations, indicating an unstable printing process. Under this condition, the voltage is just above the threshold voltage, thus creating perturbations that reduce the accuracy of the droplet deposition. After further increasing the voltage to 0.5 kV, a multi-jet was formed at the nozzle tip (as shown in figure 4(d)), indicating another form of instability. In the multi-jet printing, the applied voltage was much higher than the threshold voltage, and the printed droplets were spreading over the container. The multi-jet process can produce fine droplets of less than 2 μm, but it was unsuitable for the drop-on-demand printing required for 3D structure fabrication.

Unlike conventional EHD printing, increasing pressure will increase the ink flow rate, and droplets with a larger size and higher printing frequency can be obtained. Figure 5(a) also shows droplet sizes under different pressures with various voltages. A one-way ANOVA was used to evaluate the effect of the pressure on the droplet size. The result ($p > 0.05$) indicated that in the embedded EHD printing, pressure did not have a statistically significant effect on the droplet diameter within the selected range.

The goal of this work is to fabricate magnetic microspheres through a simple process. The morphology of the magnetic microspheres was examined using SEM. Figure 6 shows the SEM images of printed PDMS-Fe magnetic microspheres with multiple orientations (front, rear, and side views). The images from different views clearly show that the shape of the printed structures is a nearly perfect sphere with a smooth surface, which is extremely difficult to obtain in the traditional nozzle-based printing process. In traditional nozzle-based printing, droplets are directly printed on the substrate. The hard surface of the substrate and the high impact speed will force the droplet to spread on the substrate [47].

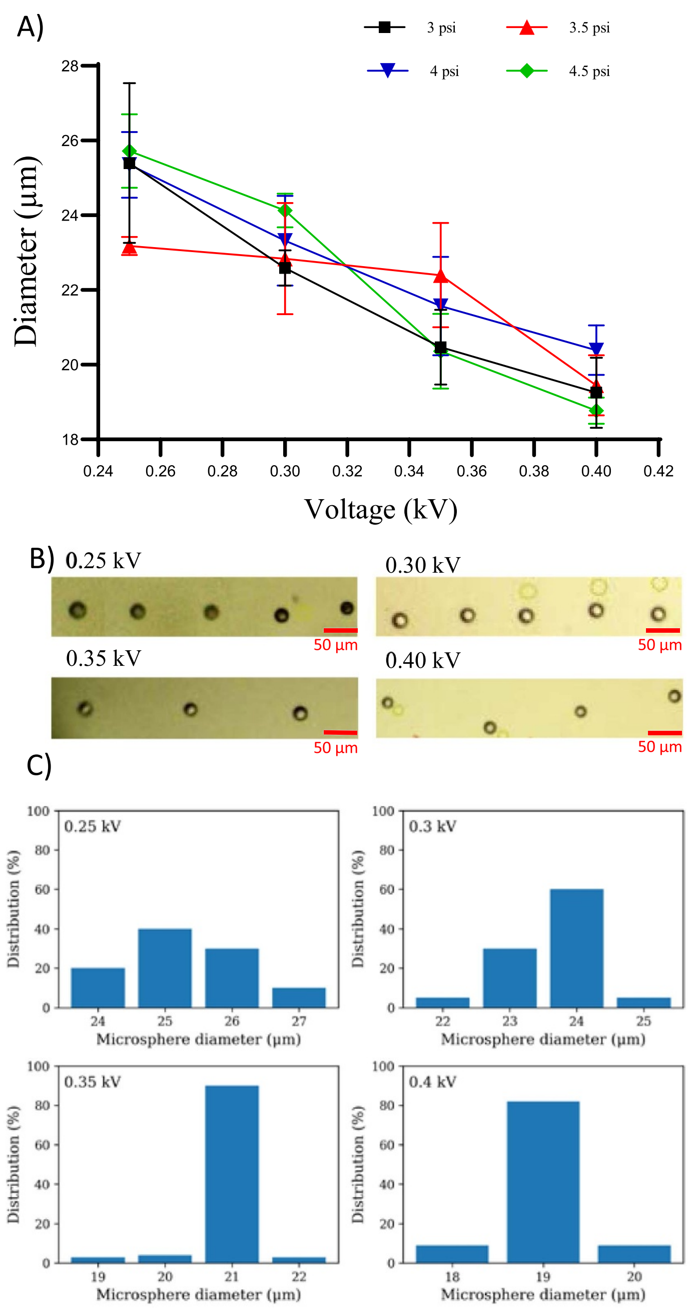

Figure 5. (a) Droplets diameter variation with variation with voltage at different values of pressures. (b) Printed microspheres at different voltages under a constant pressure of 4.5 psi. (c) Printed microsphere size histogram at different voltage under a pressure of 4.5 psi.

This spreading will prevent the droplet from forming an ideal spherical shape, even on a hydrophobic surface [48]. In embedded printing, spherical shape droplets can be easily produced. This is due to the viscosity and density of the bath material; the printed spheres will remain suspended in the bath material, which is shown in figure 7. Similar to an air bubble in water, the system naturally minimizes the surface energy; the surface tension pulls the liquid state particle into a spherical shape, which has the least surface area. Since the droplet remains suspended in the bath material, this spherical shape can be maintained until it is fully cured. However, the polydispersity in the printed microsphere size was observed, which is due to the coalescence during the prolonged printing. When printing for a time longer than 10 min, droplets in close distance (less than 5 μm) may merge together to form one larger spherical droplet before they get cured. In contrast, no aggregation is observed once the curing process is complete. In addition, the droplets in figure 7 were printed under two voltages, 0.35 and 0.40 kV, which further created some variation in microsphere size.

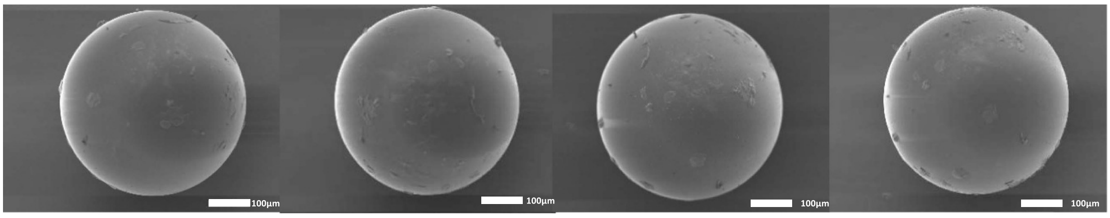

Figure 6. SEM images of a printed microsphere from different views (front, left, right and rear views respectively starting from the left).

Figure 7. Suspended microspheres (black dots) printed inside the mineral oil.

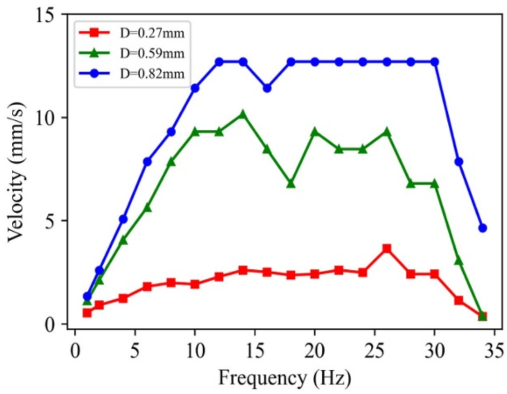

Figure 8. Velocity versus the frequency of the driving magnetic field for magnetic microspheres of different sizes.

To study the magnetic property of printed microspheres, the microspheres were driven by circularly polarized rotating magnetic fields. As the rotating magnetic field is applied to a magnetic microsphere, magnetic torque tends to align the magnetic microsphere's magnetic moment with the direction of the rotating magnetic field, which enables the magnetic microsphere to roll over the substrate. As shown in figure 8, when the frequency of the rotating magnetic field is low, the translational velocity of the magnetic microsphere is proportional to the frequency of the rotating magnetic field. When the frequency of the rotating magnetic field gets close to a critical point known as the step-out frequency (about 15 Hz for our magnetic microspheres), the magnetic microsphere stops following the rotating magnetic field; hence, its velocity drops gradually. Figure 8 shows the relationship between velocity and driving frequency of three magnetic microspheres with different sizes (0.27, 0.59, and 0.82 mm). The strength of the applied magnetic field is 5 mT. Figure 8 also clearly shows that a larger magnetic microsphere has a higher velocity than a smaller magnetic microsphere when actuated by the same magnetic field. To demonstrate the navigation capability of the magnetic microsphere under magnetic actuation, we fabricated two microchannel devices (an MSU pattern and a circular maze) using a liquid crystal display 3D printer (Anycubic Photon Mono M7). As shown in figure 9, the magnetic microsphere can be precisely navigated in these complex microchannels. The full videos of the microsphere motion are shown in Video 1 and Video 2 in the Supporting Information.

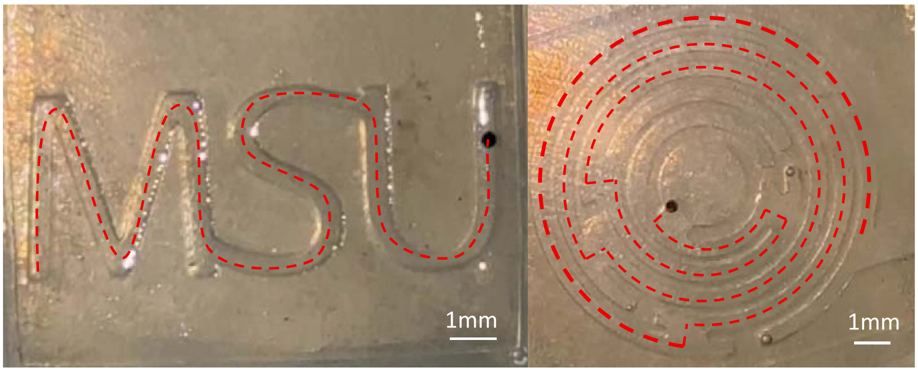

Figure 9. Navigation of a magnetic microsphere in (a) an MSU pattern and (b) a circular maze.

4. Conclusion

In this work, a novel embedded EHD printing technology has been developed to fabricate magnetic microspheres. The developed embedded EHD printing technology has been compared with the conventional EHD printing process, and a characterization test was performed to study the effect of the applied voltage and pressure on the printing behaviors and results. SEM images captured from various angles confirmed the geometric shapes and highlighted the surface texture of the magnetic microspheres. These results demonstrated that the developed embedded EHD printing process is capable of fabricating composite microspheres with well-controlled dimensions and surface texture. Magnetic actuation tests also confirmed the propulsion and precise navigation of the magnetic microspheres, showing their applications in targeted drug delivery and microsurgery. Future work can focus on measuring the actuation forces, assessing long-term stability under repeated use for a long time, and expanding the design to include more complex embedded 3D printing methods that incorporate the magnetic components into larger multifunctional systems.

Data availability statement

The data that support the findings of this study are available upon reasonable request from the authors.

Acknowledgment

This work is supported by the National Science Foundation under Grant Awards CMMI-2340414, OIA-2429775, and IOS 2200200.

Conflict of interest

There are no conflicts to declare.

Author contributions

Prashant Ghimire 0009-0005-1315-3940
Data curation (equal), Formal analysis (equal), Investigation (equal), Methodology (supporting), Validation (equal), Visualization (equal), Writing – original draft (equal), Writing – review & editing (supporting)

Augustus Kitchens
Data curation (supporting), Formal analysis (supporting), Investigation (supporting), Validation (supporting)

Kishwat Ijaz Malik
Data curation (equal), Validation (equal), Visualization (equal)

Yueheng Lin
Data curation (supporting), Validation (supporting), Visualization (supporting), Writing – review & editing (supporting)

Yongjian Qiu 0000-0002-1799-6305
Conceptualization (equal), Funding acquisition (equal), Methodology (equal), Writing – review & editing (equal)

Yang Cao 0000-0001-9209-3897
Conceptualization (equal), Funding acquisition (equal), Investigation (equal), Methodology (equal), Project administration (equal), Resources (equal), Supervision (equal), Writing – original draft (equal), Writing – review & editing (equal)

Yiwei Han 0000-0002-3876-5063
Conceptualization (equal), Funding acquisition (equal), Methodology (equal), Project administration (equal), Resources (equal), Supervision (equal), Writing – review & editing (equal)

References

[1] Ullrich F, Bergeles C, Pokki J, Ergeneman O, Erni S, Chatzipirpiridis G, Pané S, Framme C and Nelson B J 2013 Mobility experiments with microrobots for minimally invasive intraocular surgery *Invest. Ophthalmol. Vis. Sci.* **54** 2853–63
[2] Romero-velez G, Robles I, Jiménez J, Cabrera C, Luengas R, Portenier D and Kroh M 2022 Robotic magnetic surgery: results from the first prospective clinical trial *Ann. Surg. Open* **3** e225
[3] Dagnino G and Kundrat D 2024 Robot-assistive minimally invasive surgery: trends and future directions *Int. J. Intell. Robot. Appl.* **8** 812–26
[4] Yan X *et al* 2017 Multifunctional bohybrid magnetite microrobots for imaging-guided therapy *Sci. Robot.* **2** eaaq1155
[5] Nguyen K T *et al* 2021 A magnetically guided self-rolled microrobot for targeted drug delivery, real-time x-ray imaging, and microrobot retrieval *Adv. Healthcare Mater.* **10** e2001681
[6] Lee H, Kim D-I, Kwon S-H and Park S 2021 Magnetically actuated drug delivery helical microrobot with magnetic nanoparticle retrieval ability *ACS Appl. Mater. Interfaces* **13** 19633–47
[7] Cao Y, Michel K N, Alimardani F and Wang Y 2024 A review on recent progress of biodegradable magnetic microrobots for targeted therapeutic delivery: materials, structure designs, and fabrication methods *J. Micro Nano Sci. Eng.* **12**
[8] Li J, Li X, Luo T, Wang R, Liu C, Chen S, Li D, Yue J, Cheng S-H and Sun D 2018 Development of a magnetic microrobot for carrying and delivering targeted cells *Sci. Robot.* **3** eaat8829
[9] Kim S, Qiu F, Kim S, Ghanbari A, Moon C, Zhang L, Nelson B J and Choi H 2013 Fabrication and characterization of magnetic microrobots for three-dimensional cell culture and targeted transportation *Adv. Mater.* **25** 5863–8
[10] Jeon S, Park S H, Kim E, Kim J-Y, Kim S W and Choi H 2021 A magnetically powered stem cell-based microrobot for minimally invasive stem cell delivery via the intranasal pathway in a mouse brain *Adv. Healthcare Mater.* **10** e2100801
[11] Noh S *et al* 2022 A biodegradable magnetic microrobot based on gelatin methacrylate for precise delivery of stem cells with mass production capability *Small* **18** e2107888
[12] Choi J, Hwang J, Kim J-Y and Choi H 2021 Recent progress in magnetically actuated microrobots for targeted delivery of therapeutic agents *Adv. Healthcare Mater.* **10** e2001596
[13] Hou Y, Wang H, Fu R, Wang X, Yu J, Zhang S, Huang Q, Sun Y and Fukuda T 2023 A review on microrobots driven by optical and magnetic fields *Lab Chip* **23** 848–68
[14] Go J and Hart A J 2016 A framework for teaching the fundamentals of additive manufacturing and enabling rapid innovation *Addit. Manuf.* **10** 76–87
[15] Huang J, Qin Q and Wang J 2020 A review of stereolithography: processes and systems *Processes* **8** 1138
[16] Singh D, Mahendar T and Reddy A R 2021 Powder bed fusion process: a brief review *Mater. Today* **46** 350–5
[17] Saadi M A S R, Maguire A, Pottackal N T, Thakur M S H, Ikram M M, Hart A J, Ajayan P M and Rahman M M 2022 Direct ink writing: a 3D printing technology for diverse materials *Adv. Mater.* **34** e2108855
[18] Mwema F M and Akinlabi E T 2020 Basic of fused deposition modeling (FDM) *SpringerBriefs in Applied Sciences and Technology* (Springer)
[19] Schaffner M, Faber J A, Pianegonda L R, Coulter F and Studart A R 2018 3D printing of robotiv soft actuators with programmable bioinspired architectures *Nat. Commun.* **9**
[20] Ahn B Y, Duoss E B, Motala M J, Guo X, Park S-I, Xiong Y, Yoon J, Nuzzo R G, Rogers J A and Lewis J A 2009 Omnidirectional printing of flexible, stretchable, and spanning silver microelectrodes *Science* **323** 5921
[21] Sun K, Wei T-S, Ahn B Y, Seo J Y, Dillon S J and Lewis J A 2013 3D printing of interdigitated Li-ion microbattery architectures *Adv. Mater.* **25** 4539–43
[22] Compton B G and Lewis J A 2014 3D-printing of lightweight cellular composites *Adv. Mater.* **26** 5930–5
[23] Nune S K, Gunda P, Thallapally P K, Lin Y-Y, Forrest M L and Berkland C J 2009 Nanoparticles for biomedical imaging *Expert Opin. Drug Deliv.* **6** 1175–94
[24] Talebloo N, Gudi M, Robertson N and Wang P 2020 Magnetic particle imaging: current applications in biomedical research *J. Magn. Reson. Imaging* **51** 1659–68
[25] Jin Y, Compaan A, Chai W and Huang Y 2017 Functional nanoclay suspension for printing-then-solidification of liquid materials *ACS Appl. Mater. Interfaces* **9** 20057–66
[26] Zhao D, Liu Y, Liu B, Chen Z, Nian G, Qu S and Yang W 2021 3D printing method for tough multifunctional particle-based double-network hydrogels *ACS Appl. Mater. Interfaces* **13** 13714–23

[27] Zhang Y, Huang F, Zhang E and Zhang L 2023 Effect of the support bath on embedded 3D printing of soft elastomeric composites *Mater. Lett.* **331** 133475
[28] Alioglu M A, Singh Y P, Nagamine M, Rizvi S H A, Pal V, Gerhard E M, Saini S, Kim M H and Ozbolat I T 2023 3D embedded printing of microfluidic devices using a functional silicone composite support bath *Addit. Manuf.* **70** 103566
[29] Gao Z, Yin J, Liu P, Li Q, Zhang R, Yang H and Zhou H 2023 Simultaneous multi-material embedded printing for 3D heteregenous structures *Int. J. Extreme Manuf.* **5** 035001
[30] Grosskopf A K, Truby R L, Kim H, Perazzo A, Lewis J A and Stone H A 2018 Viscoplastic matrix materials for embedded 3D printing *ACS Appl. Mater. Interfaces* **10** 23353–61
[31] Turby R L, Wehner M, Grosskopf A K, Vogt D M, Uzel S G, Wood R J and Lewis J A 2018 Soft somatosensitive actuators via embedded 3D printing *Adv. Mater.* **30**
[32] Luo G, Yu Y, Yuan Y, Chen X, Liu Z and Kong T 2019 Freeform, reconfigurable embedded printing of all-aqueous 3D architectures *Adv. Mater.* **31**
[33] Wu Q, Song K, Zhang D, Ren B, Sole-gras M, Huang Y and Yin J 2022 Embedded extrusion printing in yield-stress-fluid baths *Matter* **5** 3775–806
[34] Han Y and Dong J 2018 Electrohydrodynamic printing for advanced micro/nanomanufacturing: current progresses, opportunities, and challenges *J. Micro Nanomanuf.* **6** 0408011–4080110
[35] Mkhize N and Bhaskaran H 2022 Electrohydrodynamic jet printing: introductory concepts and considerations *Small Sci.* **2** 2100073
[36] Hassan R, Sharipov M and Ryu W 2024 Electrohydrodynamic (EHD) printing of nanomaterial composite inks and their applications *Micro Nano Syst. Lett.* **12**
[37] Gao D and Zhou J G 2019 Designs and applications of electrohydrodynamic 3D printing *Int. J. Bioprint.* **5** 172
[38] Hoath S D, Hsiao W-K, Jung S, Martin G D, Hutchings I M, Morrison N F and Harlen O G 2013 Drop speeds from drop-on-demand ink-jet print heads *J. Imaging Sci. Technol.* **57** 10503–1–10503–11
[39] Mishra S, Barton K L, Alleyne A G, Ferreira P M and Rogers J A 2010 High-speed and drop-on-demand printing with a pulsed electrohydrodynamic jet *J. Micromech. Microeng.* **20** 095026
[40] Hill A and Carrington S 2006 *Understanding the Links between Rheology and Particle Parameters* (American Laboratory) p 0111
[41] Leone G, Consumi M, Pepi S, Pardini A, Bonechi C, Tamasi G, Donati A, Rossi C and Magnani A 2019 Modified low molecular weight poly-vinyl alcohol as viscocity enhancer *Mater. Today Commun.* **21** 100634
[42] Zhang Y, Chen K, Cao L, Li K, Wang Q, Fu E and Guo X 2019 Stabilization of pickering emulsions by hairy nanoparticles bearing polyanions *Polymers* **11** 816
[43] Han Y, Wei C and Dong J 2014 Super-resolution electrohydrodynamic (EHD) 3D printing of micro-structures using phase-chase inks *Manuf. Lett.* **2** 96–99
[44] Park J, Park J-W, Nasrabadi A M and Hwang J 2016 Methodology to set up nozzle-to-substrate gap for high resolution electrohydrodynamic jet printing *Appl. Phys. Lett.* **109** 134104
[45] Haque S, Lee S, Son S and Choi J 2014 A study of influence of dielectric constant of substrates in electrohydrodynamic printing *Seoul Int. Conf. Appl. Sci. Eng.* **248** 345–50
[46] Gao D, Yao D, Leist S K, Fei Y and Zhou J 2018 Mechanicsms and modeling of electrohydrodynamic phenomena *Int. J. Bioprint.* **5** 166
[47] Han Y, Wei C and Dong J 2015 Droplet formation and settlement of phase-change ink in high resolution electrohydrodynamic (EHD) 3D printing *J. Manuf. Process.* **20** 485–91 (available at: https://www.sciencedirect.com/science/article/pii/S152661251500064X)
[48] Jiang L, Huang Y, Zhang X and Qin H 2020 Electrohydrodynamic inkjet printing of polydimethylsiloxane (PDMS) *Proc. Manuf.* **48** 90–94